High Cortical Spreading Depression Susceptibility and Migraine-Associated Symptoms in $Ca_V2.1$ S218L Mice

Arn M. J. M. van den Maagdenberg, PhD,[1,2] Tommaso Pizzorusso, PhD,[3] Simon Kaja, PhD,[2,4] Nicole Terpolilli, MD,[5] Maryna Shapovalova, PhD,[6,7] Freek E. Hoebeek, PhD,[8] Curtis F. Barrett, PhD,[1,2] Lisa Gherardini, PhD,[3] Rob C. G. van de Ven, PhD,[1] Boyan Todorov, MS, PharmD,[1] Ludo A. M. Broos, BSc,[1] Angelita Tottene, PhD,[6,7] Zhenyu Gao, MSc,[8] Mariann Fodor, PhD,[9]‡ Chris I. De Zeeuw, MD, PhD,[8,10] Rune R. Frants, PhD,[1] Nikolaus Plesnila, PhD,[5] Jaap J. Plomp, PhD,[2,4] Daniela Pietrobon, PhD,[6,7] and Michel D. Ferrari, MD, PhD[2]

Objective: The *CACNA1A* gene encodes the pore-forming subunit of neuronal $Ca_V2.1$ Ca^{2+} channels. In patients, the S218L *CACNA1A* mutation causes a dramatic hemiplegic migraine syndrome that is associated with ataxia, seizures, and severe, sometimes fatal, brain edema often triggered by only a mild head trauma.
Methods: We introduced the S218L mutation into the mouse *Cacna1a* gene and studied the mechanisms for the S218L syndrome by analyzing the phenotypic, molecular, and electrophysiological consequences.
Results: *Cacna1a*^{S218L} mice faithfully mimic the associated clinical features of the human S218L syndrome. S218L neurons exhibit a gene dosage–dependent negative shift in voltage dependence of $Ca_V2.1$ channel activation, resulting in enhanced neurotransmitter release at the neuromuscular junction. *Cacna1a*^{S218L} mice also display an exquisite sensitivity to cortical spreading depression (CSD), with a vastly reduced triggering threshold, an increased propagation velocity, and frequently multiple CSD events after a single stimulus. In contrast, mice bearing the R192Q *CACNA1A* mutation, which in humans causes a milder form of hemiplegic migraine, typically exhibit only a single CSD event after one triggering stimulus.
Interpretation: The particularly low CSD threshold and the strong tendency to respond with multiple CSD events make the S218L cortex highly vulnerable to weak stimuli and may provide a mechanistic basis for the dramatic phenotype seen in S218L mice and patients. Thus, the S218L mouse model may prove a valuable tool to further elucidate mechanisms underlying migraine, seizures, ataxia, and trauma-triggered cerebral edema.

ANN NEUROL 2010;67:85–98

Published online in Wiley InterScience (www.interscience.wiley.com). DOI: 10.1002/ana.21815

Received Oct 22, 2008, and in revised form Jul 8, 2009. Accepted for publication Jul 28, 2009.

Address correspondence to Dr van den Maagdenberg, Department of Human Genetics, Leiden University Medical Centre, Einthovenweg 20, PO Box 9600, Leiden, The Netherlands. E-mail: maagdenberg@lumc.nl For CNS electrophysiology, Dr Pietrobon, Department of Biomedical Sciences, University of Padova, Viale G. Colombo 3, 35121 Padova, Italy. E-mail: daniela.pietrobon@unipd.it.

Current address for Dr Kaja: Department of Ophthalmology, University of Missouri–Kansas City, School of Medicine, Kansas City, MO.

From the Departments of [1]Human Genetics and [2]Neurology, Leiden University Medical Centre, Leiden, The Netherlands; [3]Department of Psychology, University of Firenze and CNR Institute of Neuroscience, Pisa, Italy; [4]Department of Molecular Cell Biology–Section Neurophysiology, Leiden University Medical Centre, Leiden, The Netherlands; [5]Department of Neurosurgery and Institute for Surgical Research, University of Munich Medical Centre–Grosshadern, Munich, Germany; [6]Department of Biomedical Sciences, University of Padova; [7]CNR Institute of Neuroscience, Padova, Italy; [8]Department of Neuroscience, Erasmus Medical Centre, Rotterdam; [9]Department of Embryology and Anatomy, Leiden University Medical Centre, Leiden; and [10]Netherlands Institute for Neuroscience, Royal Dutch Academy for Sciences (KNAW), Amsterdam, The Netherlands.

‡Dr Mariann Fodor is deceased.

A.M.J.M.v.d.M., T.P., S.K., and N.T. contributed equally to this article.

Additional Supporting Information may be found in the online version of this article.

Familial hemiplegic migraine (FHM) is an autosomal dominant subtype of migraine in which attacks are associated with transient hemiparesis and other neurological aura symptoms.[1] We consider FHM a valid monogenic model for studying pathogenetic mechanisms that are involved in the genetically more complex common forms of migraine. The arguments here for this are mainly clinical and include: (1) the headache and aura features of FHM and common migraine attacks are, apart from the hemiparesis, identical; (2) two-thirds of FHM patients have, in addition to attacks of FHM, attacks of common nonhemiplegic migraine; (3) two thirds of their first-degree relatives have attacks of common nonhemiplegic migraine; (4) both FHM and common migraine attacks can be precipitated by similar trigger factors and can be prevented with the same prophylactic agents; and (5) their headache phases can be aborted with the same acute treatments.[2–5]

FHM has been linked to three genes, all of which encode proteins that drive or regulate neuronal excitability (see Van den Maagdenberg and colleagues[6] and Pietrobon[7] for review). FHM1 is caused by mutations in the *CACNA1A* gene[6–10] that encodes the α_{1A}-subunit of neuronal $Ca_V2.1$ (P/Q-type) voltage gated calcium channels, which couple presynaptic Ca^{2+} entry to synaptic neurotransmitter release.[11] Functional studies in heterologous expression systems support a net gain-of-function effect of FHM1 mutations[12–16] (but see also Cao and colleagues,[17,18] and Barrett and colleagues[19]). In an analysis of the single-channel properties of eight different FHM1 mutations, open probability (and therefore integrated Ca^{2+} current) was increased over a broad voltage range, as a consequence of a shift to lower voltages for channel activation.[12–14] Consistent with these findings, cerebellar granule and cortical pyramidal neurons from knock-in mice carrying the FHM1 R192Q mutation exhibited significantly increased P/Q-type current density at negative voltages.[20,21] These mice also showed enhanced excitatory transmission at cortical synapses caused by increased action potential–evoked Ca^{2+} influx and increased probability of glutamate release,[21] and as a consequence, a decreased triggering threshold for cortical spreading depression (CSD).[20,21] CSD is a slowly propagating wave of cortical neuronal and glial depolarization that underlies the migraine aura[22] and may possibly activate migraine headache mechanisms.[23]

Although the *CACNA1A*^{R192Q}, and most other FHM1 mutations, cause only mild forms of FHM, which are not associated with additional major neurological features,[7,8,24] the *CACNA1A*^{S218L} FHM1 mutation causes a particularly dramatic clinical syndrome. This "S218L syndrome" consists of, in addition to attacks of hemiplegic migraine, slowly progressive cerebellar ataxia, epileptic seizures, and severe, sometimes fatal, cerebral edema which can be triggered by only a trivial head trauma.[25–28]

To understand how a single amino acid substitution can account for such a wide range of neurological features, we generated transgenic knock-in mice bearing the S218L missense mutation in the *Cacna1a* gene, and examined the clinical and functional consequences of the mutation. This provides a unique opportunity to study shared pathogenetic mechanisms, not only for FHM and common migraine, but also for cerebellar ataxia, epilepsy, and mild head trauma–triggered cerebral edema, each of which has also been linked with common types of migraine.[29–35]

We found that *Cacna1a*^{S218L} mice indeed display the main associated clinical features of the human "S218L syndrome." In addition, these mice exhibit a number of important neurobiological changes. These changes include: (1) highly increased neuronal Ca^{2+} influx through $Ca_V2.1$ channels; (2) strongly increased spontaneous release of neurotransmitter at the neuromuscular junction (NMJ); and (3) a dramatically reduced triggering threshold for CSD, with an increased propagation velocity and an increased probability of multiple CSD events on a single stimulation. We believe that the unique vulnerability to CSD may explain many of the dramatic features of the S218L syndrome. Moreover, the *Cacna1a*^{S218L} mouse may prove a valuable tool to study shared pathogenetic mechanisms of brain disorders that may model or are frequently co-occurring with common types of migraine.

Materials and Methods

Generation of Transgenic Cacna1a^{S218L} *Mice*

The generation of *Cacna1a*^{R192Q} mice was described previously.[19] The *Cacna1a* gene was modified to generate *Cacna1a*^{S218L} mice using a gene-targeting approach such that exon 5 contained the human FHM1 S218L mutation. In the targeting vector, the original TCA triplet codon 218 was changed into TTA by site-directed mutagenesis, creating the S218L mutation. Upstream of exon 5, a PGK-driven neomycin cassette flanked by LoxP sites was introduced. E14 strain embryonic stem cells were electroporated, and positive clones were screened for homologous recombination by Southern blot analysis using the external probes indicated in Figure 1A. The presence of the S218L mutation was confirmed by polymerase chain reaction (PCR) amplification of exon 5 using primers 271 (5′-CTCCATGGGAGGCACTTG-3′) and 272 (5′-ACCTGTCCCCTCTTCAAAGC-3′), and subsequent digestion with restriction enzyme *Vsp*I, as well as direct sequencing of the PCR products. Correctly targeted embryonic stem cells were injected into C57Bl/6J blastocysts to create chimeric animals. Offspring that were heterozygous for the S218L+Neo allele were crossed with EIIA-*Cre* deleter mice[36] to

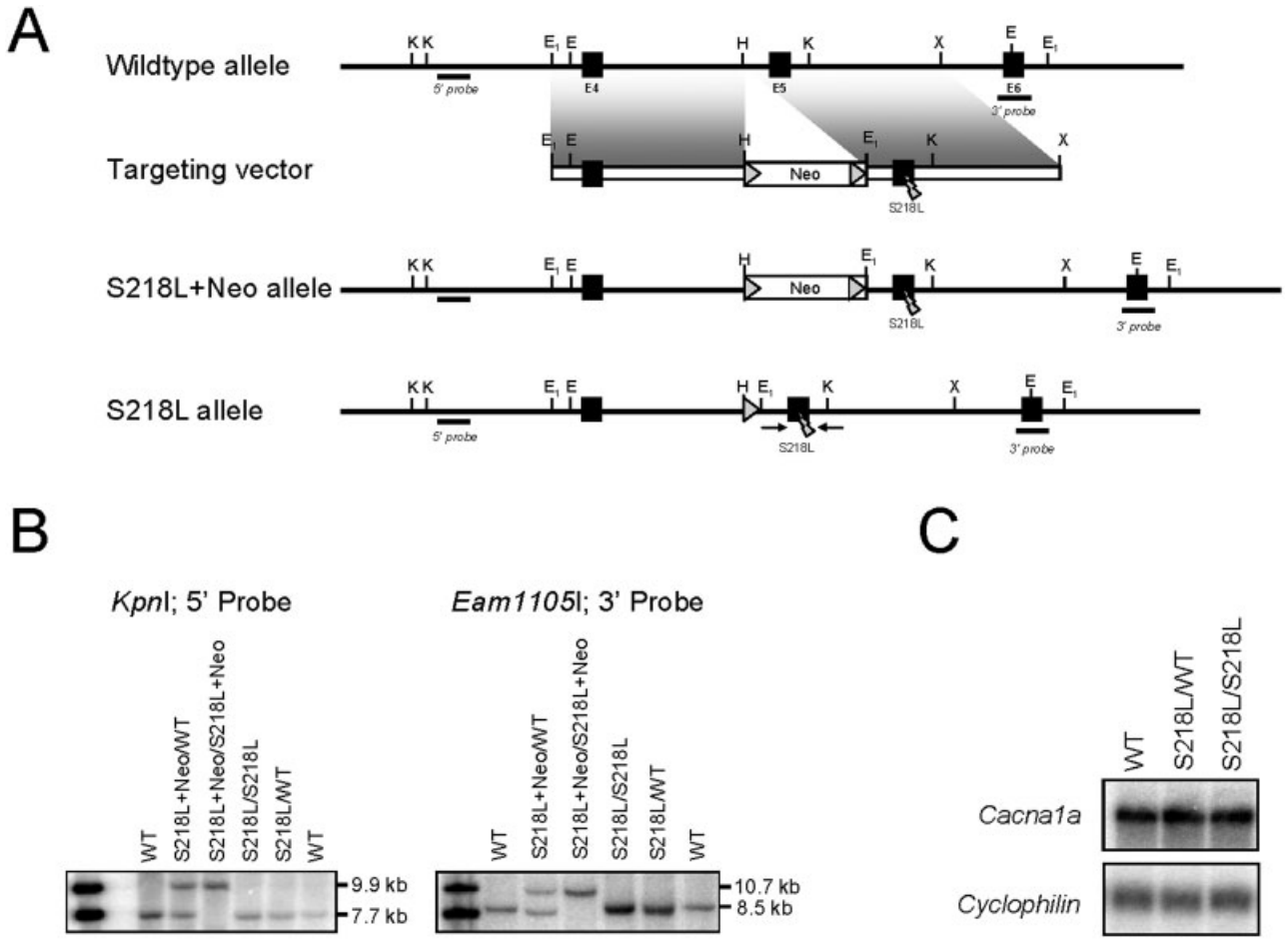

FIGURE 1: Generation of *Cacna1a*^{S218L} knock-in mice. (A) Genomic structure of the wild-type (WT) *Cacna1a* allele, targeting vector and predicted structure after homologous recombination (S218L+Neo allele), and after Cre-mediated deletion of the neomycin cassette (S218L allele). LoxP sites are indicated by *triangles. Black numbered boxes* indicate respective exons, with the S218L mutation in E5. *Thick black lines* indicate probes for Southern blot analysis. Primers used for genotyping and confirmation of the S218L mutation are depicted schematically with *arrows.* Restriction sites: E, *Eam1105*I; E_1, *Eco*RI; H, *Hind*III, K, *Kpn*I; X, *Xba*I. (B) Southern blot for all genotypes of S218L+Neo and S218L allele carriers showing genomic DNA digested with *Kpn*I or *Eam1105*I and tested with the 5′ or 3′ probe, respectively. (C) Northern blot of adult WT, *Cacna1a*$^{S218L/WT}$, and *Cacna1a*$^{S218L/S218L}$ brains. Total brain RNA was hybridized with *Cacna1a* and *Cyclophilin* complementary DNA probes. Note that *Cacna1a* message levels are similar among genotypes.

excise the neomycin cassette. *Cacna1a*^{S218L} mice in which the neomycin cassette was successfully deleted were backcrossed to C57Bl/6Jico mice. *Cacna1a*$^{S218L/WT}$, *Cacna1a*$^{S218L/S218L}$, and wild-type (WT) littermates of the third generation were used for all analyses (approximately 87.5% C57Bl/6Jico and approximately 12.5% 129Ola background). Genotyping of mice for all experiments was performed by PCR analysis as described earlier. All animal experiments were performed in accordance with the guidelines of the respective institutions and national legislation. The studies were performed using a similar number of male and female mice, and summary data show results from both sexes. For all experiments, the investigator was blinded to the genotype.

RNA Analysis

For RNA extraction, mice were killed by cervical dislocation, and forebrain and cerebellum were dissected in ice-cold phosphate-buffered saline (pH 7.4) and subsequently snap frozen in liquid nitrogen. For Northern blot and reverse transcriptase PCR experiments, RNA was isolated as described previously.[19] For Northern blot analysis, 10μg cerebellar RNA was separated on a 1% agarose gel and subsequently transferred to a Hybond-N+ membrane (Amersham Biosciences, Buckinghamshire, United Kingdom). ^{32}P-labeled PCR products of *Cacna1a* or *Cyclophilin* complementary DNA were used as probes using standard hybridization and washing conditions.

Rotarod

The accelerating Rotarod (UGO Basile S.R.L., Commerio VA, Italy) test was performed on a 4cm diameter horizontal rotating rod. The test was performed in a semidark room with a light source placed at the bottom to discourage the mice from jumping off the Rotarod. Mice (8–10 weeks of age) were tested in groups of five. After a training period (in which the mice were

placed on the Rotarod turning at a low constant speed of 5 rpm for 5 minutes), the mice were subjected to 6 consecutive days of trials (1 trial per day). Each trial started with the Rotarod turning at a constant speed of 5 rpm for 10 seconds, after which the speed was gradually increased to 45 rpm over the following 5 minutes. The latency to fall (ie, endurance) was recorded, and the endurance per trial per genotype is presented as mean ± standard error of the mean.

Electroencephalography

Electroencephalographic (EEG) electrodes were surgically implanted under isoflurane anesthesia in 10- to 14-week-old mice. Six 1mm diameter stainless-steel screw electrodes were positioned as follows: one in each frontal bone and one in each medial bone for recording activity patterns from primary motor and parietal cortices, respectively. The remaining two electrodes (placed in the temporal bone) served as reference (medial) and ground (lateral) electrodes. Isolated copper wire was used to attach the electrodes to a mini-connector that was cemented to the skull with dental acrylic. Recording began 2 hours after surgery. For recording, animals were placed in an electrically shielded sound-proof box for continuous EEG recording and simultaneous video observation. Electrical signals were amplified, filtered (CyberAmp, Molecular Devices, Sunnyvale, CA), digitized (1401Plus; Cambridge Electronic Design, Cambridge, United Kingdom), and stored for off-line analysis (Spike2; Cambridge Electronic Design). Differential EEG signals were sampled at 500Hz and filtered using a bandpass of 0.1 to 30Hz. The behavior of the mice was continuously monitored with a video camera and recorded at 25 frames per second using custom-made software (Labview; National Instruments, Austin, TX). Recording lasted up to 48 hours, during which food and water were available ad libitum.

Survival Analysis

Survival curves were constructed using the method of Kaplan and Meier.[37] The survival curves were compared by the log-rank test. Survival times were calculated from the date of birth to the date of death. Mice that died of unknown cause (ie, not related to an experimental intervention) were considered cases. Statistical analysis was performed using SPSS 10.0 software (SPSS, Chicago, IL).

In Vivo Model of Cerebral Impact and Quantification of Brain Edema

Anesthesia was initiated in an isoflurane chamber (4%) and was maintained thereafter with 1.5% isoflurane in 30% oxygen/68.5% nitrous oxide supplied by a face mask. Mild impact was induced essentially as described previously,[38] but with the important difference that the *intensity* of the weight drop was considerably diminished by reducing the height from where the weight was dropped from 72 to 15cm. Whereas a weight drop from 72cm causes severe neurological deficits and high mortality (>30%) in WT mice, the modified low-height mild-impact protocol did not cause mortality or any obvious neurological dysfunction in WT mice. In brief, the animal's head was fixed in a stereotactic frame and the skull was exposed by a midline incision. Body temperature was kept constant at 37°C using a feedback-controlled heating pad connected to a rectal probe (Heater Control Module; FHC, Bowdoinham, ME). Impact to the brain was applied by dropping a 72gm weight guided through a plastic tube onto the skull from a height of 15cm. Immediately after the impact the skin was closed and animals were transferred to an incubator heated to 35°C until recovery of spontaneous motor activity (30 minutes). Brain water content was determined as described previously.[39,40] In brief, 24 hours after impact, mice were killed and the brains were removed. After removal of the cerebellum and olfactory bulb, the brains were weighed to obtain their wet weight (ww), dried at 110°C for 24 hours, and then reweighed to obtain their dry weight (dw). Brain water content (expressed as percentage) was calculated using this formula: $((ww - dw)/ww) \cdot 100$.

$Ca_V2.1$ Current in Cerebellar Granule Cells

Cerebellar granule cells were grown in primary culture from 6-day-old mice as described previously.[41] Experiments were performed on cells grown from 6 to 7 days in vitro. Whole-cell patch-clamp recordings were performed at room temperature as described previously.[20,41] The external recording solution contained (in mM): $BaCl_2$ 5, tetraethylammonium-Cl 148, Hepes 10, 0.1mg/ml cytochrome *c,* pH 7.4 with tetraethylammonium-OH. The internal solution contained (in mM): Cs-methanesulfonate 100, $MgCl_2$ 5, Hepes 30, EGTA 10, adenosine triphosphate 4, guanosine triphosphate 0.5 and cyclic adenosine monophosphate 1, pH 7.4 with CsOH. Currents were low-pass filtered at 1kHz and digitized at 5kHz. Compensation (typically 70%) for series resistance was generally used. Current-voltage (*I-V*) relationships were obtained only from cells with a voltage error of less than 5mV and without signs of inadequate space clamping such as notchlike current discontinuities, slow components in the decay of capacitive currents (in response to hyperpolarizing pulses), or slow tails not fully inhibited by nimodipine. The average normalized *I-V* curves were multiplied by the average maximal current density obtained from all cells. *I-V* curves were fitted with the equation $I_{Ba} = G \cdot (V - E_{rev})/(1+e\text{^}((V_{0.5} - V)/k))$ using a nonlinear regression method based on the Levenberg–Marquardt algorithm. The liquid junction potentials were such that a value of 12mV should be subtracted from all voltages to obtain the correct values of membrane potential in whole-cell recordings.[41] All drugs were stored as stock solutions at −20°C: 250μM ω-conotoxin-GVIA (ω-CgTx-GVIA; Bachem, Budendorf, Switzerland) and 250μM ω-conotoxin-MVIIC (ω-CTx-MVIIC; Bachem) in distilled water, 10mM nimodipine (a gift from Dr Hof, Sandoz, Basel, Switzerland) in 95% ethanol.

Ex Vivo Neuromuscular Junction Electrophysiology

The NMJ is a model synapse in the peripheral nervous system exclusively relying on presynaptic $Ca_v2.1$ channels[42] and can be electrophysiologically analyzed with relative ease to investigate neurotransmission. Mice (approximately 2 months of age) were

killed by carbon dioxide inhalation. Phrenic nerve hemidiaphragms were dissected and mounted at room temperature in standard Ringer's medium containing (in mM) NaCl 116, KCl 4.5, $CaCl_2$ 2, $MgSO_4$ 1, NaH_2PO_4 1, $NaHCO_3$ 23, glucose 11, pH 7.4. The solution was continuously bubbled with 95% O_2/5% CO_2.

Intracellular recordings of miniature end-plate potentials (MEPPs; the small, spontaneous depolarizing events caused by uniquantal acetylcholine release) and end-plate potentials (EPPs; the depolarization resulting from nerve action potential–evoked acetylcholine release) were performed at NMJs at 28°C using standard microelectrode equipment as described previously.[43,44] At least 30 MEPPs and EPPs were recorded at each NMJ, and typically 7 to 15 NMJs were sampled per experimental condition per muscle. Muscle action potentials were prevented with the muscle-specific sodium channel blocker μ-conotoxin-GIIIB (3μM; Scientific Marketing Associates, Barnet, Herts, United Kingdom). EPPs were recorded in Ringer's medium as described earlier except containing 0.2mM Ca^{2+}. The nerve was electrically stimulated with 100μs supramaximal pulses delivered at 0.3Hz. Amplitudes of EPPs and MEPPs were normalized to −75mV, assuming 0mV as the reversal potential for acetylcholine-induced current.[45] The normalized EPP amplitudes were corrected for nonlinear summation[46] with an f value of 0.8. The quantal content at each NMJ (ie, the number of acetylcholine quanta released per nerve impulse) was calculated by dividing the normalized, corrected mean EPP amplitude by the normalized mean MEPP amplitude.

Cortical Spreading Depression

For CSD experiments, *Cacna1a*^{S218L}, and for comparison *Cacna1a*^{R192Q}, transgenic and WT mice (20–30g) were anesthetized with urethane (20% in saline; 6ml/kg intraperitoneally). The mice were mounted in a stereotaxic apparatus and continuously monitored for adequate level of anesthesia, temperature, heart rate, and lack of nociceptive reflexes. Three holes were drilled in the skull over the left hemisphere to record CSD. The first corresponded to the occipital cortex and was used for access of the electrical stimulation electrode. The second hole, at the parietal cortex (1mm lateral and 1mm caudal to Bregma), and the third hole, at the frontal cortex (1mm lateral and 1mm rostral to Bregma), were used for placement of the recording electrodes. The dura was carefully removed from a small part of the cortex using a 28-gauge needle from a small part of the cortex, sufficient to let the recording electrode (tip diameter, 3μm) enter the cortex. The steady-state (direct current) potential was recorded with glass micropipettes placed 200μm below the dural surface. An Ag/AgCl reference electrode was placed subcutaneously above the nose. Cortical stimulation was conducted using a copper bipolar electrode placed on the cortex after removing the dura. Pulses of increasing intensity (from 10 up to 800μA) were applied for 100 milliseconds at 3-minute intervals with a stimulus isolator/constant current unit (WPI, Sarasota, FL) until a CSD event was observed. The minimal stimulus intensity at which a CSD event was elicited was taken as the CSD threshold. Once a CSD event was elicited, the recording continued for 1 hour without stimulation, and additional CSD events were noted. The percentage of mice with multiple CSD events was determined only from those mice that could be recorded for 1 full hour after the first detected event. In some WT mice, the CSD induction threshold was reassessed at the end of the 1-hour monitoring of recurrent CSDs and found to be unchanged from the initial threshold, suggesting that the general recording conditions remain stable for at least 1 hour. To measure CSD propagation velocity, we divided the distance between the two recording electrodes by the time elapsed between the CSD onset at the first and second recording sites. The condition of the cortex was monitored using a surgical microscope, and animals with lesions were excluded.

Statistical Analysis

Statistical differences were analyzed with paired or unpaired Student's t test, analysis of variance with Tukey's HSD post hoc test, Fisher's exact test, repeated-measures analysis of variance, or Kruskal–Wallis one-way analysis of variance on ranks followed by Dunn's comparison procedure as post hoc test, all where appropriate. Calculations were performed with a statistical software package (SigmaStat 3.0, Erkrath, Germany). For all experiments, summary data are presented as mean ± standard error of the mean; $p < 0.05$ was considered to be statistically significant.

Results

Generation of the S218L Knock-in Mice

Using a gene-targeting approach with homologous recombination, we introduced the human *CACNA1A*^{S218L} mutation into the orthologous *Cacna1a* gene (see Figs 1A, B) to generate *Cacna1a*^{S218L} mice. Both RNA (see Fig 1C) and protein analyses (see Supplementary Fig 1) indicated that neither the mutation nor the introduction of the LoxP site appeared to have interfered with any major regulatory sequence because no major effect on *Cacna1a* expression with respect to quantity or location was observed. However, the experiments were not designed to demonstrate minor differences in *Cacna1a* expression.

S218L Mice Exhibit Main Features of the Human S218L Syndrome

Cacna1a$^{S218L/S218L}$ mice showed a complex neurological phenotype that is remarkably similar to that of what is seen in *CACNA1A*^{S218L} patients (Fig 2A). Most of the time, the mice appeared phenotypically normal, except for mild cerebellar ataxia. The ataxia was reflected by poor performance in the Rotarod test (see Fig 2B), accompanied by reduced arborization solely of proximal, primary dendrites of cerebellar Purkinje neurons (see Fig 2C and Supplementary Fig 2A). These primary dendrites in *Cacna1a*$^{S18L/S218L}$ had a decreased length (see Supplementary Fig 2B). Purkinje cells of 2-month-old S218L mice showed abnormal distal turns and a "weeping willow" ap-

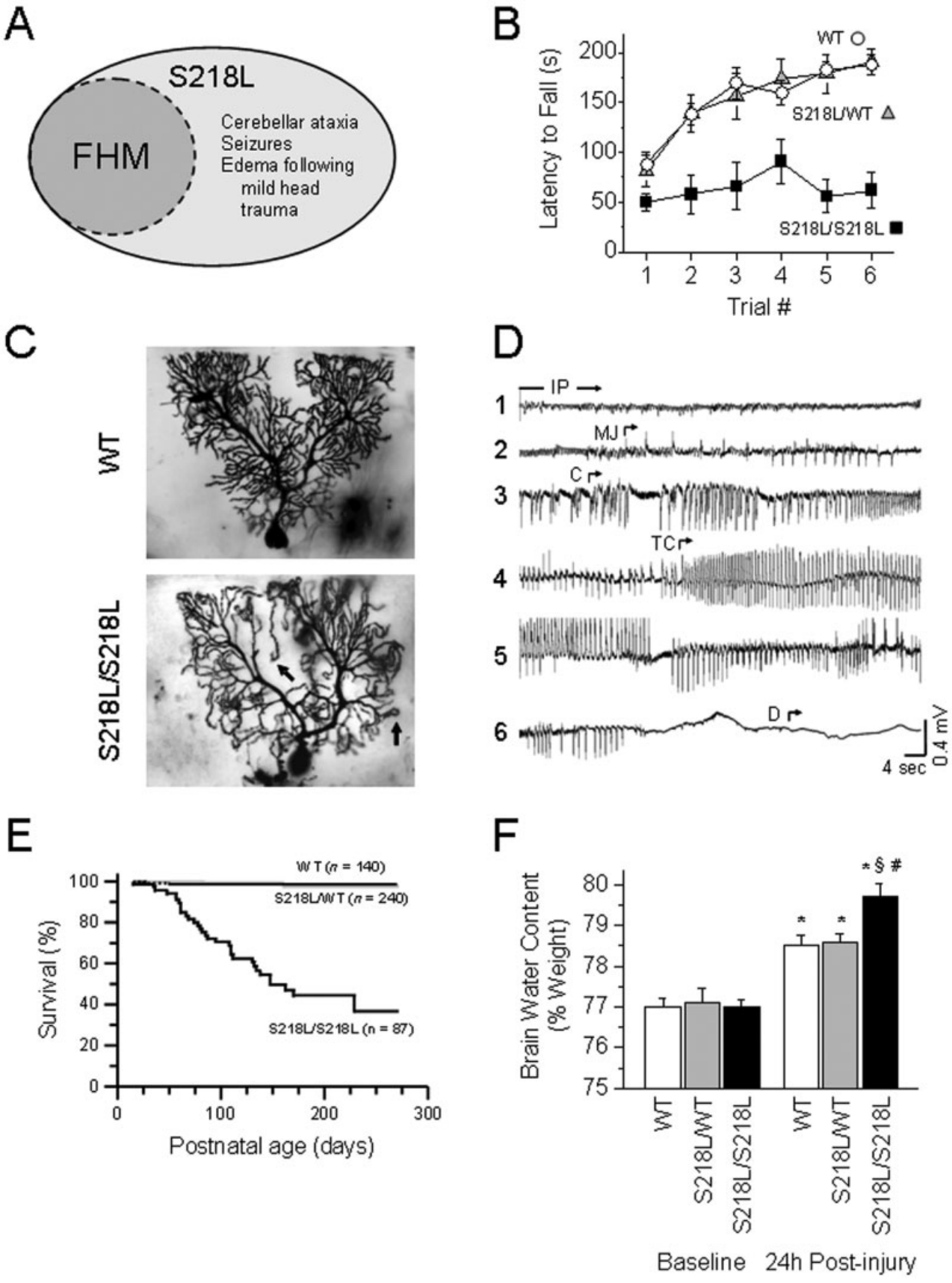
A
S218L
FHM
Cerebellar ataxia
Seizures
Edema following
mild head
trauma
B
Latency to Fall (s)
200
150
100
50
0
WT
S218L/WT
S218L/S218L
1
2
3
4
5
6
Trial #
C
WT
S218L/S218L
D
IP
MJ
C
TC
D
1
2
3
4
5
6
0.4 mV
4 sec
E
WT (n = 140)
S218L/WT (n = 240)
S218L/S218L (n = 87)
Survival (%)
100
80
60
40
20
0
0
100
200
300
Postnatal age (days)
F
Brain Water Content
(% Weight)
80
79
78
77
76
75
*
*
* § #
WT
S218L/WT
S218L/S218L
WT
S218L/WT
S218L/S218L
Baseline
24h Post-injury

FIGURE 2.

pearance (see Fig 2C) similar to what has been reported for aged (>1 year) *Rocker* mice, which carry the naturally occurring *Cacna1a*^{T1310K} missense mutation.[47]

We observed two types of spontaneous attacks in *Cacna1a*$^{S218L/S218L}$ mice: (1) attacks of hemiparesis, which are consistent with the attacks of hemiparesis as seen in S218L FHM1 patients; and (2) attacks of generalized seizures that were fatal in some cases. The hemiparetic attacks consisted of brief periods of apparent transient unilateral weakness, manifesting as slow, circular locomotion (because of leg movement only on one side of the body) and attempts to support themselves against the cage wall on the side of the hemiparesis. After such episodes, the mouse would remain immobile for about 20 minutes and then recovered. Some of these attacks were captured on video (see Supplementary movie for an example). In addition to the hemiparetic attacks, we also observed attacks that started with myoclonic jerks and subsequently evolved into generalized tonic-clonic ("grand mal") seizures. We were able to capture and analyze several of such episodes in three mice with EEG recording coupled to video monitoring (see Fig 2D; see also Supplementary note 1). All three mice died at the end of such an episode.

In line with the observation that mice can die after spontaneous epileptic attacks, the life expectancy of *Cacna1a*$^{S218L/S218L}$ mice, kept in their home cage environment (without experimental interventions), was significantly decreased (see Fig 2E). Postmortem analysis indicated that the likely cause of death was lung edema, a frequent finding in epilepsy-related deaths, often secondary to cardiac arrest (data not shown). Pathological examination excluded myocardial infarction, or other morphological abnormalities, in these cases. Additional histology of homozygous S218L brain material at the light microscope level did not demonstrate obvious structural abnormalities such as neurodegeneration (data not shown). The earlier-described spontaneous episodes of hemiparesis, fatal seizures, and reduced life expectancy all appear to be unique to *Cacna1a*$^{S218L/S218L}$ mice; none was observed in *Cacna1a*$^{S218L/WT}$ (see Fig 2) or in mice carrying the R192Q mutation (*Cacna1a*$^{R192Q/R192Q}$), which in patients is associated with a much milder form of hemiplegic migraine.[7]

Consistent with observations in S218L patients, *Cacna1a*$^{S218L/S218L}$ mice, but not WT or *Cacna1a*$^{S218L/WT}$ mice, exhibited significant brain edema 24 hours after mild head impact as applied in our modified low-height weight-drop model (see Fig 2F). The brain water content increased by only 1.51% in WT mice (from 76.99 $\pm$ 0.67 to 78.50 $\pm$ 1.14%) and by only 1.49% in *Cacna1a*$^{S218L/WT}$ mice (from 77.12 $\pm$ 0.94 to 78.61 $\pm$ 1.07%). In contrast, in *Cacna1a*$^{S218L/S218L}$ mice, the brain water content increased significantly by 2.84% (from 76.89 $\pm$ 0.64 to 79.73 $\pm$ 0.93 %; $p < 0.02$ vs *Cacna1a*$^{S218L/WT}$ and WT mice). Baseline brain water content was similar in all three genotypes. Twenty percent of the *Cacna1a*$^{S218L/S218L}$ mice, but none of the WT or *Cacna1a*$^{S218L/WT}$ mice, died after these mild impact experiments.

Taken together, these results demonstrate that *Cacna1a*$^{S218L/S218L}$ mice faithfully mimic the broad spectrum of spontaneous episodic, mild impact-triggered, and permanent clinical features seen in S218L patients.

Gain-of-Function Effect on Whole-Cell Ca^{2+} Influx and Synaptic Transmission

To understand the molecular consequences of the S218L mutation on $Ca_V2.1$ channel functioning, we performed whole-cell patch-clamp recordings of cerebellar granule neurons (Fig 3A). Neurons expressing S218L channels displayed significantly increased whole-cell $Ca_V2.1$ current density at negative voltages as reflected by a pronounced gene dosage–dependent leftward shift in voltage-dependent activation (see Fig 3B). In contrast, current density was not changed at positive voltages, indicating that the number of functional $Ca_v2.1$ channels at the somatodendritic plasma membrane is similar across genotypes (see also Supplementary note 2). Moreover, the enhanced Ca^{2+} influx was not accompanied by significant changes in the density of other high-voltage–activated Ca_V channels, except for a slight decrease in L-type currents (see Fig 3C).

FIGURE 2: Phenotypic consequences in *Cacna1a*^{S218L} mice. (A) Venn diagram depicting the overlapping and distinct clinical characteristics of pure familial hemiplegic migraine (FHM), as well as the "S218L syndrome" with severe associated features exhibited in S218L patients. (B) Rotarod testing for ataxia in 2-month-old mice shows severe impairments in both performance and learning for *Cacna1a*$^{S218L/S218L}$ mice (n = 10–11). Trials were performed on consecutive days. (C) Golgi-Cox staining of cerebellar Purkinje neurons from 2-month-old wild-type (WT) and *Cacna1a*$^{S218L/S218L}$ mice. *Arrows* indicate decreased branching and downturned ends in the *Cacna1a*$^{S218L/S218L}$ neuron. (D) Long-term electroencephalographic recording of a *Cacna1a*$^{S218L/S218L}$ mouse showing sequential phases (1–6) of a "grand mal" fatal seizure. Concurrent video monitoring was used to assess the overt clinical phenotype, described as follows: IP, interictal period; MJ, myoclonic jerks; C, clonic seizure, TC, tonic-clonic seizure; D, death. (E) Kaplan–Meier plot showing significantly decreased survival of *Cacna1a*$^{S218L/S218L}$ mice ($p < 0.001$ vs WT). (F) Twenty-four hours after mild head impact (see Materials and Methods), *Cacna1a*$^{S218L/S218L}$ mice had increased cerebral water content (n = 9, 15, and 5 mice for WT, *Cacna1a*$^{S218L/WT}$, and *Cacna1a*$^{S218L/S218L}$, respectively; *$p < 0.05$ vs WT; #$p < 0.05$ vs S218L/WT).

The effects in *Cacna1a*$^{S218L/S218L}$ neurons were reminiscent of the changes seen in neurons of the clinically milder R192Q mice,[20] but were more pronounced. As a consequence of the even lower activation threshold of S218L channels,[14] the gain-of-function of the $Ca_V2.1$ current at low voltages was more dramatic in *Cacna1a*$^{S218L/S218L}$ neurons than the gain-of-function we previously observed in *Cacna1a*$^{R192Q/R192Q}$ neurons, leading to Ca^{2+} influx close to the resting potential. While the $Ca_V2.1$ current at −40mV was approximately 4 times larger in *Cacna1a*$^{R192Q/R192Q}$ neurons compared with WT neurons,[20] the $Ca_V2.1$ current in *Cacna1a*$^{S218L/S218L}$ neurons was 6.6 times larger than that in WT neurons (see Fig 3B).

Consistent with Ca^{2+} influx occurring close to the resting potential, the S218L mutation produced a much larger increase in the frequency of spontaneous transmitter release events (ie, the MEPPs) at the NMJ when compared with the R192Q mutation. While the MEPP frequency in *Cacna1a*$^{R192Q/R192Q}$ mice was only 2.5 times greater than in WT mice,[20] the MEPP frequency in *Cacna1a*$^{S218L/WT}$ mice was 8.5 times and in *Cacna1a*$^{S218L/S218L}$ mice 12.5 times greater in comparison with WT mice (Fig 4A).

Remarkably, although a similar increase in $Ca_V2.1$ current at −40mV, relative to their respective WT mice,

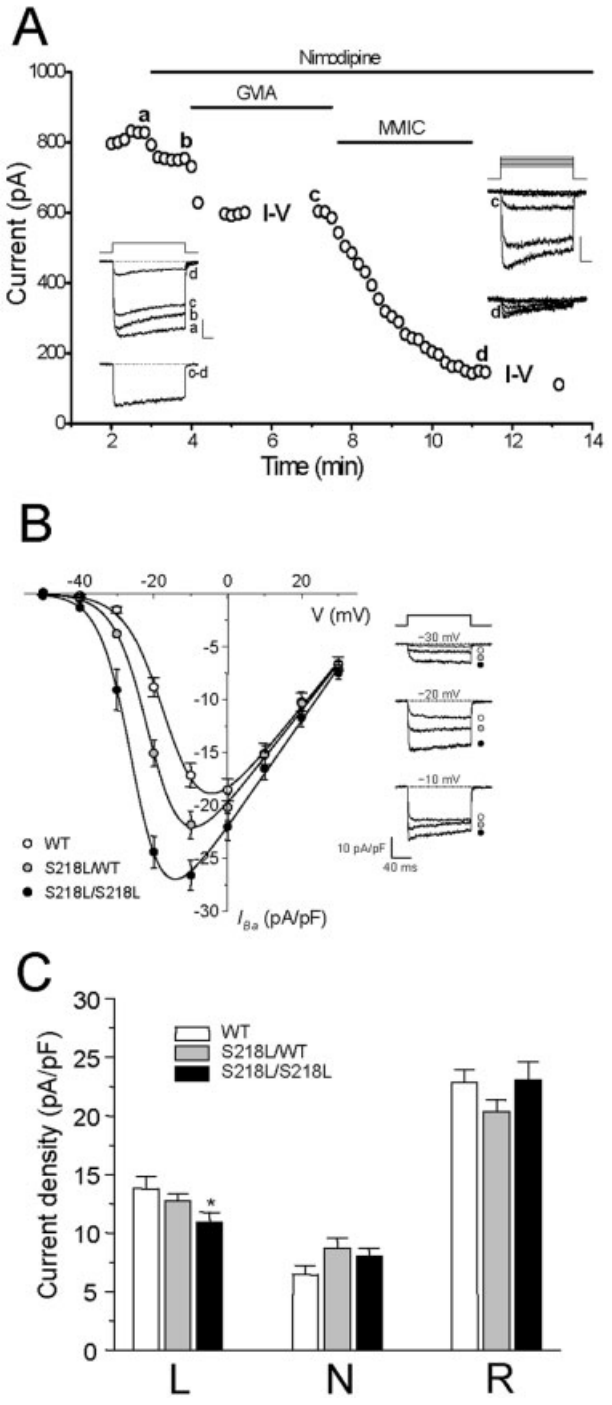

FIGURE 3: $Ca_V2.1$ (P/Q-type) current density (I_{Ba}) is increased in cerebellar granule neurons from *Cacna1a*^{S218L} mice. (A) Peak amplitude of whole-cell Ba^{2+} current recorded from a *Cacna1a*$^{S218L/WT}$ cerebellar granule cell in primary culture during successive step depolarizations to −10mV that were applied at 10-second intervals from a holding potential of −80mV (5mM Ba^{2+} as the charge carrier). Nimodipine (5μM), ω-conotoxin GVIA (1μM), and ω-conotoxin MVIIC (3μM) were applied to the bath as indicated. (left inset) Representative current traces taken at times *a, b, c, d* and difference trace representing the $Ca_V2.1$ (P/Q-type) component (*c-d*). (right inset) Representative traces at increasing voltage from −50 to −10mV, measured at I-V *c* and I-V *d*. Scale bars = 20 milliseconds, 200pA. (B) $Ca_V2.1$ current density as a function of voltage in wild-type (WT; *white circles*), *Cacna1a*$^{S218L/WT}$ *(gray circles),* and *Cacna1a*$^{S218L/S218L}$ mice *(black circles).* The $Ca_V2.1$ current was isolated pharmacologically as shown in (A). Peak whole-cell P/Q-type Ba^{2+} currents were divided by the membrane capacitance, normalized to their maximal value, and averaged; average normalized *I-V* curves (n = 14, 12, and 10 cells for WT, *Cacna1a*$^{S218L/WT}$, and *Cacna1a*$^{S218L/S218L}$, respectively) were multiplied by the average maximal current densities (n = 35, 44, and 28 cells, respectively). Individual *I-V* curves were fit with the equation $I_{Ba} = G \cdot (V - E_{rev})/(1+e\text{^}((V_{0.5} - V)/k))$. Average (± standard error of the mean) $V_{0.5}$ values were −15 ± 1 (WT), −20.1 ± 0.8 (*Cacna1a*$^{S218L/WT}$; $p < 0.005$ vs WT), and −25 ± 1mV (*Cacna1a*$^{S218L/S218L}$; $p < 0.005$ vs *Cacna1a*$^{S218L/WT}$, $p < 0.00005$ vs WT). (inset) P/Q-type Ba^{2+} currents elicited at the voltages indicated (pooled from different cells). (C) Current densities of L-, N-, and R-type Ca^{2+} channels in WT and *Cacna1a*^{S218L} mice, measured at −10mV. The different current types were isolated pharmacologically as shown in (A). The current densities for the L-type component were 10.5 ± 0.7 (n = 24), 12.7 ± 0.7 (n = 27), and 13.8 ± 1.1 (n = 29) pA/pF in *Cacna1a*$^{S218L/S218L}$ *(black bars),* *Cacna1a*$^{S218L/WT}$ *(gray bars),* and WT neurons *(white bars),* respectively; current densities for the N-type were 8.0 ± 0.7 (n = 27), 8.8 ± 0.8 (n = 29), and 6.5 ± 0.8 (n = 29) pA/pF; current densities for the R-type were 23.0 ± 1.6 (n = 28), 20.4 ± 1.0 (n = 43), and 22.9 ± 1.1 (n = 35) pA/pF. The sum of the three components (total non-$Ca_V2.1$ current density) was similar for all three genotypes (41.5 ± 1.9, 41.9 ± 1.5, and 43.2 ± 1.7pA/pF).

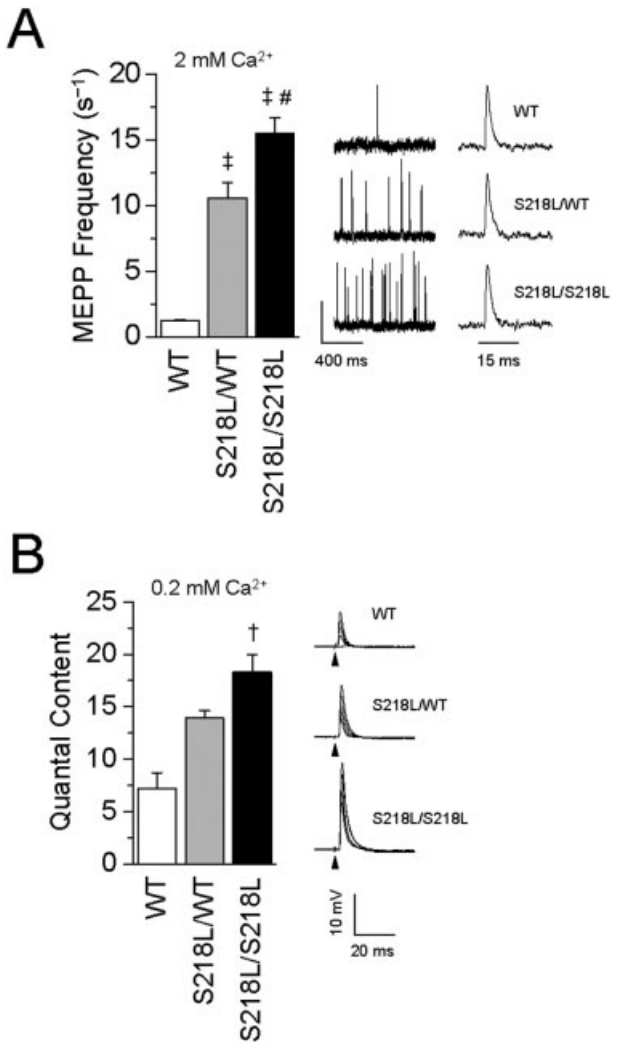

FIGURE 4: Synaptic transmission at the neuromuscular junction (NMJ). Synaptic transmission at the NMJ is increased in *Cacna1a*^{S218L} mice. (A) Summary of miniature end-plate potential (MEPP) frequency (n = 6; ‡p < 0.001 vs wild-type [WT]; #p < 0.01 vs *Cacna1a*$^{S218L/WT}$). Exemplar recordings are shown at the right. Vertical scale bar = 0.75mV. (B) Summary of neurotransmitter release in 0.2mM extracellular Ca^{2+} evoked by supramaximal stimulation of the phrenic nerve (n = 3 mice; †p < 0.01 vs WT). At the right are exemplar end-plate potentials. *Black triangles* mark the stimulation moment.

was measured in cerebellar granule neurons from *Cacna1a*$^{S218L/WT}$ (2.7 times larger; see Fig 3B) and *Cacna1a*$^{R192Q/R192Q}$ mice (3.8 times larger[20]), the relative increase in MEPP frequency was much greater in *Cacna1a*$^{S218L/WT}$ mice, consistent with more Ca^{2+} influx at rest in *Cacna1a*$^{S218L/WT}$ nerve terminals. However, quantal content (ie, the number of neurotransmitter quanta released by an action potential) measured in low extracellular Ca^{2+} was 2.5 times increased in S218L synapses (compared with WT; see Fig 4B) to a similar extent as in R192Q synapses (3.4 times compared with WT[20]). This observation suggests a ceiling effect for release probability at the NMJ.

Extreme Susceptibility of S218L Mice for Cortical Spreading Depression

Because CSD is the likely underlying mechanism for migraine aura,[22] and has also been implicated in epilepsy and edema,[48] increased susceptibility for CSD in S218L compared with R192Q mice could explain many features of the dramatic S218L syndrome. To test this hypothesis, we assessed the triggering threshold for CSD, the CSD propagation velocity, and the probability of multiple CSD events on a single stimulus in the two knock-in mouse models.

Indeed, S218L mice showed both a lower threshold for CSD induction (Fig 5A; for examples of CSD traces, see Supplementary Fig 3) and a faster propagation of CSD waves (see Fig 5B) compared with R192Q mice. In addition, S218L mice had a gene dosage–dependent increased probability of experiencing successive CSD events on a single stimulus: the probability was the greatest in homozygous *Cacna1a*$^{S218L/S218L}$ mice, which carry two copies of the S218L allele, lowest in WT mice, and in between in heterozygous *Cacna1a*$^{S218L/WT}$ mice, which carry only one copy of the S218L allele (see Fig 5C). There was, however, no difference in average latency until the first recurrent CSD between *Cacna1a*$^{S218L/WT}$ (1,323 ± 189 seconds) and *Cacna1a*$^{S218L/S218L}$ (1,108 ± 211 seconds) (p = 0.35).

It is noteworthy to emphasize that, although CSD induction threshold and propagation velocity are similar in *Cacna1a*$^{S218L/WT}$ and *Cacna1a*$^{R192Q/R192Q}$ mice (see Figs 5A, B), multiple CSD events were seen only rarely in *Cacna1a*$^{R192Q/R192Q}$ mice (see Fig 5C).

The selectively high incidence of multiple CSDs in S218L mice makes it unlikely that recurring CSDs would be merely caused by tissue damage during CSD recordings. If tissue damage had been the underlying cause, one would have expected a more evenly distributed increased probability of repetitive CSD events over the various genotypes. In contrast, R192Q mice hardly exhibited recurring CSD events. Lastly, great care was taken in monitoring the condition of the cortex. Mice with visible cortical lesions, as identified using a surgical microscope, were excluded from the analyses.

Discussion

Here, we present the generation and behavioral, electrophysiological, and neurobiological characterization of S218L knock-in mice bearing the human pathogenic *CACNA1A*^{S218L} missense mutation in $Ca_V2.1$ calcium channels. In humans, this mutation causes a broad and

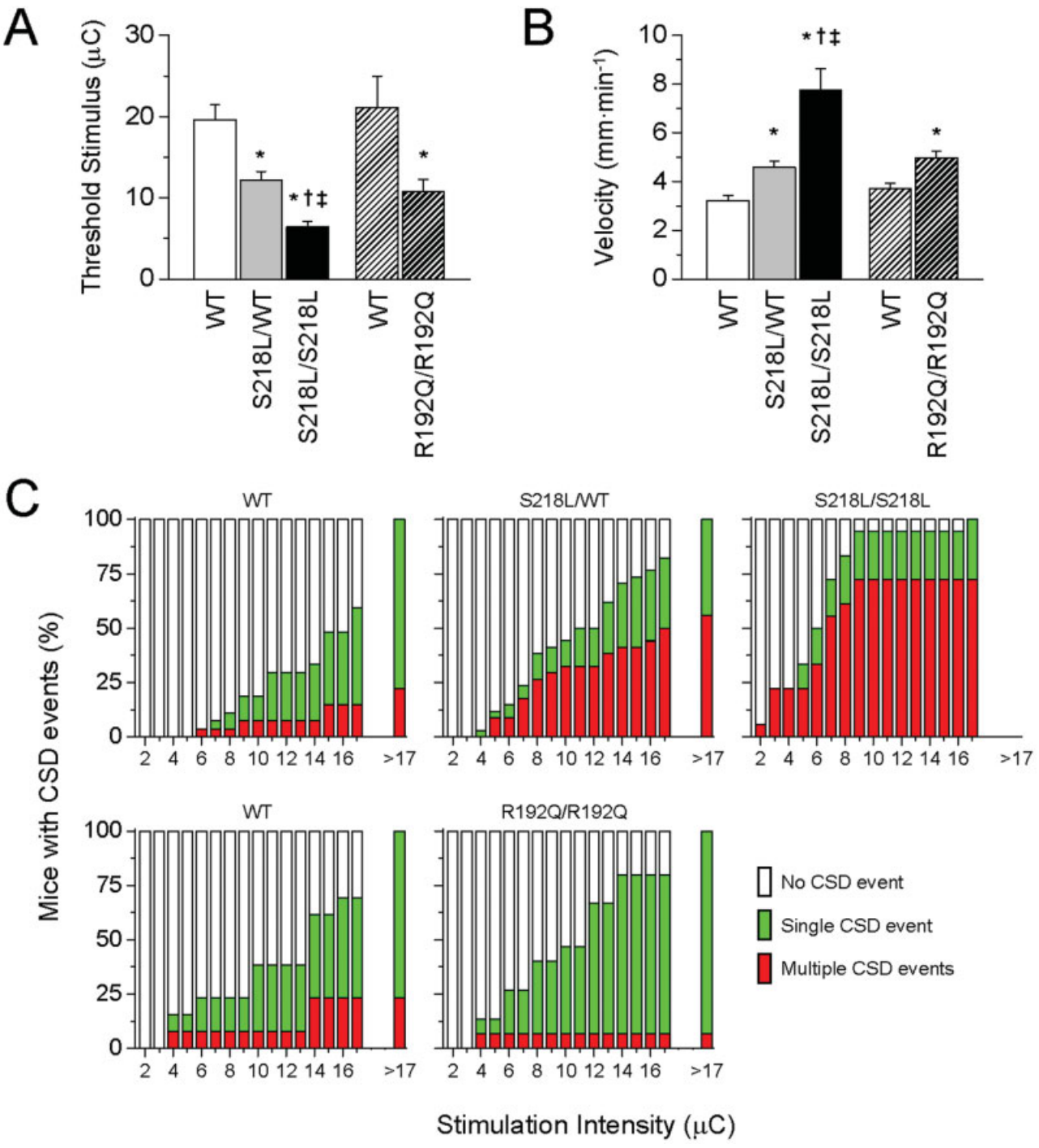

FIGURE 5: Increased susceptibility to cortical spreading depression (CSD) in *Cacna1a*^{S218L} and *Cacna1a*^{R192Q} mice. (A) Summary of the threshold required to elicit at least one CSD event in wild-type (WT), *Cacna1a*^{S218L}, and *Cacna1a*^{R192Q} mice. *Cacna1a*^{S218L} strain: n = 30, 39, and 22 mice for WT, *Cacna1a*$^{S218L/WT}$, and *Cacna1a*$^{S218L/S218L}$, respectively. *Cacna1a*^{R192Q} strain: n = 28 and 31 mice for WT and *Cacna1a*^{R192Q}, respectively. *$p < 0.05$ versus WT; †$p < 0.05$ versus S218L/WT; ‡$p < 0.05$ versus R192Q/R192Q. (B) Summary of CSD velocity measured using two recording electrodes (see Materials and Methods). Sample sizes are as in (A). *$p < 0.05$ versus WT; †$p < 0.05$ versus S218L/WT; ‡$p < 0.05$ versus R192Q/R192Q. (C) Proportion of mice (expressed as a percentage of all mice) with no response, a single CSD, or multiple CSD events as a function of stimulation intensity. *Cacna1a*^{S218L} strain: n = 27, 34, and 18 mice for WT, *Cacna1a*$^{S218L/WT}$, and *Cacna1a*$^{S218L/S218L}$, respectively. *Cacna1a*^{R192Q} strain: n = 13 and 15 mice for WT and *Cacna1a*^{R192Q}, respectively.

devastating, sometimes even fatal, clinical syndrome, with both episodic and progressive features of brain dysfunction. In this respect, the S218L syndrome is at the very extreme of the clinical spectrum of migraine. Our findings can be summarized as follows: First, S218L mice display a complex phenotype consisting of mild permanent cerebellar ataxia, spontaneous attacks of hemiparesis and/or (sometimes fatal) seizures, and brain edema after only a mild head impact. These features faithfully mimic the clinical spectrum of patients carrying the *CACNA1A*^{S218L} mutation.[25–28]

Second, most of the functional consequences of the S218L mutation are qualitatively similar to, but quantitatively more pronounced, than those of the R192Q mutation; this correlates well with the milder phenotype that is seen in patients with the R192Q mutation[8] and strongly supports the view that these changes are causally relevant. Specifically, when compared with *Cacna1a*$^{R192Q/R192Q}$ neurons[20,21,44] (and this study), *Cacna1a*$^{S218L/S218L}$ neurons have: (1) a greater increase in $Ca_V2.1$-mediated Ca^{2+} current density on weak depolarization; (2) a larger increase in spontaneous neurotransmitter release at the NMJ, a model synapse in the peripheral nervous system that relies exclusively on $Ca_V2.1$ channels and can be electrophysiologically analyzed with relative ease; and (3) a greater susceptibility for CSD, as reflected by a lower triggering threshold, higher propagation velocity, and a higher probability of successive CSD events on only a single stimulus (see also later). Moreover, heterozygous *Cacna1a*$^{S218L/WT}$ and homozygous *Cacna1a*$^{R192Q/R192Q}$ mice showed quantitatively similar gain-of-function effects in Ca^{2+} current density, and CSD threshold and velocity. However, spontaneous neurotransmitter release at the NMJ was much larger in *Cacna1a*$^{S218L/WT}$ mice, suggesting a larger Ca^{2+} influx at rest in nerve terminals.

In contrast with the good correlation between severity of the phenotype and facilitation of both neuronal Ca^{2+} current and CSD, the facilitation of evoked release at the NMJ at low extracellular [Ca^{2+}] was similar in *Cacna1a*$^{S218L/S218L}$ and *Cacna1a*$^{R192Q/R192Q}$ mice. In fact, at physiological extracellular [Ca^{2+}], evoked release at the NMJ of both mutant mice[20] (also data not shown) was not different from that at WT NMJs. Tottene and colleagues[21] reported an enhanced evoked glutamate release at excitatory cortical pyramidal cell synapses of *Cacna1a*$^{R192Q/R192Q}$ mice at physiological [Ca^{2+}], but an unaltered evoked GABA release from inhibitory fast-spiking interneuron synapses (despite being also controlled by $Ca_V2.1$ channels). Thus, the NMJ may perhaps be a better model for cortical inhibitory fast-spiking interneuron synapses than cortical excitatory synapses, whose gain-of-function was shown to be causally linked to CSD facilitation.[21]

Third, the S218L FHM1 mutation, but not the R192Q FHM1 mutation, increased the probability of multiple CSD events in response to only a single threshold stimulus. Whereas WT and R192Q mice generally experienced a single CSD event on a single stimulus, the S218L mice showed a gene dosage–dependent increased probability of having successive CSD events. This tendency of S218L mice for successive CSD events is particularly remarkable given that, despite similar CSD induction threshold and propagation velocity for *Cacna1a*$^{R192Q/R192Q}$ and *Cacna1a*$^{S218L/WT}$ mice (see Figs 5A, B), multiple CSD events are seen only rarely in *Cacna1a*$^{R192Q/R192Q}$ mice (see Fig 5C). Thus, the cortical susceptibility to repetitive CSD events is apparently unique to the S218L mutation.

The exact mechanism for recurrent CSD events after a single stimulus and the exact downstream consequences of multiple CSD events remain to be determined. The combination of the more negative activation threshold of S218L $Ca_V2.1$ channels, coupled with both their impaired inactivation during long depolarization and faster recovery from inactivation,[14] suggests the involvement of a process that is particularly sensitive to Ca^{2+} influx at rest, channel inactivation, or both. Perhaps prolonged Ca^{2+} influx during the first CSD event may be involved as well.

Our findings suggest that the high sensitivity of the S218L brain to even mild stimuli (eg, low-impact head trauma) may be explained, at least in part, by the unique combination of a particularly low CSD trigger threshold and a high propensity for multiple CSD events. Increased susceptibility to the effects of successive CSD events may also play a role. By analogy, we propose that similar mechanisms underlie the severe and clinically broad phenotype that is seen in S218L patients, but not in patients carrying other, milder FHM1 mutations. Thus, our data provide a mechanistic basis for the *overlapping* clinical manifestations of both R192Q and S218L patients, as well as for the *additional* severe clinical features seen only in S218L patients.

There is ample evidence that migraine, mild head trauma–triggered migraine attacks (such as in footballer's migraine), brain edema, epilepsy, and (subclinical) cerebellar ataxia can co-occur in various combinations.[10,29–33,48,49] This suggests shared molecular disease pathways. For instance, both migraine attacks and seizures are associated with excessive neuronal excitability in the cortex.[31] Whereas CSD is well recognized as the pathophysiological correlate of the migraine aura,[50,51] its role in epilepsy is less clear. Clearly, there is a distinction between spreading depression and hypersynchronous activity in seizures, but it appears that spreading depression may gradually evolve

into "spreading convulsions" when waves occur at high frequency.[52] Eikermann-Haerter and coworkers[53] recently showed that generalized seizures may occur 45 to 75 minutes after a single KCl-induced CSD in homozygous *Cacna1a*^{S218L} mice, but not in *Cacna1a*^{R192Q} mice, indicating that CSD and epileptic events are separated in time. Follow-up studies, comparing the exact conditions under which CSD and epilepsy may occur in $Ca_V2.1$ mutant mouse types, are likely to shed further light on the similarities and dissimilarities of these two apparently opposing neuronal mechanisms underlying episodic brain dysfunction.

CSD has also been implicated in edema.[48] In rodents, waves of spreading depression caused transient severe neuronal swelling, changes in dendritic structures,[54] and prolonged severe vascular leakage with impairment of the blood–brain barrier.[55] Opening of the blood–brain barrier, which possibly is secondary to multiple CSD events, preceded cortical edema in a patient with a severe attack of FHM type 2 caused by an *ATP1A2* mutation.[56] We, therefore, like to speculate that the unique vulnerability of the S218L brain to multiple CSD events may underlie the dramatic and sometimes fatal clinical features in both S218L patients and mice. Future experiments are needed to address the issue of whether the edema is a direct consequence of trauma, or is due to either trauma-induced CSD or epilepsy.

As yet, it is unclear how the S218L mutation may cause cerebellar ataxia. One can speculate that the ataxia may be caused by excessive Ca^{2+} influx in cerebellar Purkinje cells, to a differential effect of the mutation on the afferent inputs of Purkinje cells, or both. These mechanisms are likely to disturb the delicately regulated firing patterns of the Purkinje cells, as suggested earlier by studies in naturally occurring *Cacna1a* mouse mutants.[57,58]

Despite the advantages that our R192Q and S218L mice have to study disease mechanisms, it is also clear that the models needs further validation. For instance, it needs to be established whether R192Q and S218L mice can experience migraine attacks and whether transgenic mice are, indeed, useful models to study migraine. Although the S218L mice appear helpful in investigating how a single $Ca_V2.1$ mutation may lead to a combination of clinical phenotypes (ie, hemiplegic migraine, seizures, cerebellar ataxia, and mild head trauma induced edema) seen in FHM1 S218L patients, it is also clear that the co-occurrence of phenotypes in these mice makes it much harder to study the effect of a $Ca_V2.1$ mutation on *specific* phenotypes. In this respect, it needs to be shown that these mice will further advance our knowledge on understanding disease mechanisms of, for instance, hemiplegic migraine or cerebellar ataxia. A direct extrapolation of results from mice to patients should be done with great caution, as there are obvious differences in the physiology between humans and experimental animal models. Future studies need to show the benefits and limitations of these transgenic mouse models.

In summary, we report here that S218L FHM1 mice faithfully appear to mimic the salient clinical features of the broad human S218L hemiplegic migraine syndrome, and we propose a mechanistic explanation for these severe clinical features. Despite the limitations mentioned earlier, we believe that the S218L and R192Q knock-in FHM1 mouse models will likely serve as valuable tools to unraveling, at least to some extent, mechanisms for FHM, common migraine, epilepsy, and cerebral edema.

This work was supported by the Netherlands Organization for Scientific Research (NWO; 903-52-291, M.D.F., R.R.F.; Vici 918.56.602, M.D.F.); the EU "EUROHEAD" (LSHM-CT-2004-504837, D.P., M.D.F) and the Center of Medical System Biology established by the Netherlands Genomics Initiative/Netherlands Organisation for Scientific Research and Community (M.D.F., R.R.F., A.M.J.M.v.d.M.); Telethon Italy (GGP05236, T.P.), Italian Ministry of Education University Research (Grants PRIN2005 and FIRB2002; D.P.); the Prinses Beatrix Fonds (MAR01-0105, J.J.P.); the Hersenstichting Nederland (9F01(2).24, J.J.P.); KNAW van Leersumfonds (AFD/ML/2901, J.J.P.); the Dutch ZON-MW Organization for Medical Sciences (912-07-022, C.I.d.Z.); ALW Life Sciences, Senter (Neuro-Bsik, BSIK03053, C.I.d.Z.); Prinses Beatrix Fonds (OP05-16/100506, C.I.d.Z.); the SENSOPAC program of the European Community (028056, C.I.d.Z.); and European Molecular Biology Organization postdoctoral fellowship (ALTF810-2005, S.K.) and a Michael Smith Foundation for Health Research trainee award (ST-PDF-00140[05-1]BM, S.K.).

We thank M. L. Maat-Schieman, S. van Duijnen, and S. Verbeek for help in histological experiments and embryonic cell stem injections, and E. Hess for expert opinions on the evaluation of the behavioral phenotype. In addition, we thank E. Putignano, U. Nehrdich, and R. van der Giessen for technical assistance.

References

1. Headache Classification Subcommittee of the International Headache Society. The international classification of headache disorders: 2nd edition. Cephalalgia 2004;24:1–160.
2. Terwindt GM, Ophoff RA, Haan J, et al. Variable clinical expression of mutations in the P/Q-type calcium channel gene in familial hemiplegic migraine. Neurology 1998;50:1105–1110.

3. Ducros A, Denier C, Joutel A, et al. The clinical spectrum of familial hemiplegic migraine associated with mutations in a neuronal calcium channel. N Engl J Med 2001;345:17–24.
4. Ferrari MD, Goadsby PJ. Migraine as a cerebral ionopathy with abnormal central sensory processing. In: Gilman S, Pedley T, eds. Neurobiology of disease. New York: Elsevier, 2006:333–348.
5. Ferrari MD. Migraine. Lancet 1998;351:1043–1051.
6. Van den Maagdenberg AM, Haan J, Terwindt GM, Ferrari MD. Migraine: gene mutations and functional consequences. Curr Opin Neurol 2007;20:299–305.
7. Pietrobon D. Familial hemiplegic migraine. Neurotherapeutics 2007;4:274–284.
8. Ophoff RA, Terwindt GM, Vergouwe MN, et al. Familial hemiplegic migraine and episodic ataxia type-2 are caused by mutations in the Ca^{2+} channel gene CACNL1A4. Cell 1996;87:543–552.
9. Adams PJ, Snutch TP. Calcium channelopathies: voltage-gated calcium channels. Subcell Biochem 2007;45:215–251.
10. Stam AH, van den Maagdenberg AM, Haan J, et al. Genetics of migraine: an update with special attention to genetic comorbidity. Curr Opin Neurol 2008;21:288–293.
11. Catterall WA. Structure and function of neuronal Ca2+ channels and their role in neurotransmitter release. Cell Calcium 1998;24: 307–323.
12. Hans M, Luvisetto S, Williams ME, et al. Functional consequences of mutations in the human alpha(1A) calcium channel subunit linked to familial hemiplegic migraine. J Neurosci 1999; 19:1610–1619.
13. Tottene A, Fellin T, Pagnutti S, et al. Familial hemiplegic migraine mutations increase Ca^{2+} influx through single human CaV2.1 channels and decrease maximal $Ca_V2.1$ current density in neurons. Proc Natl Acad Sci U S A 2002;99:13284–13289.
14. Tottene A, Pivotto F, Fellin T, et al. Specific kinetic alterations of human CaV2.1 calcium channels produced by mutation S218L causing familial hemiplegic migraine and delayed cerebral edema and coma after minor head trauma. J Biol Chem 2005; 280:17678–17686.
15. Kraus RL, Sinnegger MJ, Glossmann H, et al. Familial hemiplegic migraine mutations change alpha(1A) Ca^{2+} channel kinetics. J Biol Chem 1998;273:5586–5590.
16. Kraus RL, Sinnegger MJ, Koschak A, et al. Three new familial hemiplegic migraine mutants affect P/Q-type Ca(2+) channel kinetics. J Biol Chem 2000;275:9239–9243.
17. Cao YQ, Piedras-Rentería ES, Smith GB, et al. Presynaptic Ca^{2+} channels compete for channel type-preferring slots in altered neurotransmission arising from Ca^{2+} channelopathy. Neuron 2004;43:387–400.
18. Cao YQ, Tsien RW. Effects of familial hemiplegic migraine type 1 mutations on neuronal P/Q-type Ca2+ channel activity and inhibitory synaptic transmission. Proc Natl Acad Sci U S A 2005; 102:2590–2595.
19. Barrett CF, Cao YQ, Tsien RW. Gating deficiency in a familial hemiplegic migraine type 1 mutant P/Q-type calcium channel. J Biol Chem 2005;280:24064–24071.
20. Van den Maagdenberg AM, Pietrobon D, Pizzorusso T, et al. A Cacna1a knock-in migraine mouse model with increased susceptibility to cortical spreading depression. Neuron 2004;41:701–710.
21. Tottene A, Conti R, Fabbro A, et al. Enhanced excitatory transmission at cortical synapses as the basis for facilitated spreading depression in Ca(v)2.1 knockin migraine mice. Neuron 2009;61: 762–773.
22. Lauritzen M. Pathophysiology of the migraine aura. The spreading depression theory. Brain 1994;117:199–210.
23. Bolay H, Reuter U, Dunn AK, et al. Intrinsic brain activity triggers trigeminal meningeal afferents in a migraine model. Nat Med 2002;8:136–142.
24. Haan J, Kors EE, Vanmolkot KR, et al. Migraine genetics: an update. Curr Pain Headache Rep 2005;9:213–220.
25. Fitzsimons RB, Wolfenden WH. Migraine coma. Meningitic migraine with cerebral oedema associated with a new form of autosomal dominant cerebellar ataxia. Brain 1985;108:555–577.
26. Kors EE, Terwindt GM, Vermeulen FL, et al. Delayed cerebral edema and fatal coma after minor head trauma: role of CACNA1A calcium channel subunit gene and relationship with familial hemiplegic migraine. Ann Neurol 2001;49:753–760.
27. Curtain RP, Smith RL, Ovcaric M, Griffiths LR. Minor head trauma-induced sporadic hemiplegic migraine coma. Pediatr Neurol 2006;34:329–332.
28. Chan YC, Burgunder JM, Wilder-Smith E, et al. Electroencephalographic changes and seizures in familial hemiplegic migraine patients with the CACNA1A gene S218L mutation. J Clin Neurosci 2008;15:891–894.
29. Sándor PS, Mascia A, Seidel L, et al. Subclinical cerebellar impairment in the common types of migraine: a three-dimensional analysis of reaching movements. Ann Neurol 2001;49:668–672.
30. Ambrosini A, Sándor PS, De Pasqua V, et al. Performances in cerebellar and neuromuscular transmission tests are correlated in migraine with aura. J Headache Pain 2008;9:29–32.
31. Rogawski MA. Common pathophysiologic mechanisms in migraine and epilepsy. Arch Neurol 2008;65:709–714.
32. Haan J, van den Maagdenberg AM, Brouwer OF, et al. A review of the genetic relation between migraine and epilepsy. Cephalalgia 2008;28:105–113.
33. Blau JN, Solomon F. Migraine and intracranial swelling: an experiment of nature. Lancet 1985;28:718.
34. Meaney JF, Williams CE, Humphrey PR. Case report: transient unilateral cerebral oedema in hemiplegic migraine: MR imaging and angiography. Clin Radiol 1996;51:72–76.
35. Cha YH, Millett D, Kane M, et al. Adult-onset hemiplegic migraine with cortical enhancement and oedema. Cephalalgia 2007;27:1166–1170.
36. Lakso M, Pichel JG, Gorman JR, et al. Efficient in vivo manipulation of mouse genomic sequences at the zygote stage. Proc Natl Acad Sci U S A 1996;93:5860–5865.
37. Kaplan EL, Meier P. Nonparametric estimation from incomplete observations. J Am Stat Assoc 1958;53:457–481.
38. Chen Y, Constantini S, Trembovler V, et al. An experimental model of closed head injury in mice: pathophysiology, histopathology, and cognitive deficits. J Neurotrauma 1996;13: 557–568.
39. Vakili A, Kataoka H, Plesnila N. Role of arginine vasopressin V1 and V2 receptors for brain damage after transient focal cerebral ischemia. J Cereb Blood Flow Metab 2005;25:1012–1019.
40. Zweckberger K, Erös C, Zimmermann R, et al. Effect of early and delayed decompressive craniectomy on secondary brain damage after controlled cortical impact in mice. J Neurotrauma 2006;23: 1083–1093.
41. Fletcher CF, Tottene A, Lennon VA, et al. Dystonia and cerebellar atrophy in CACNA1A null mice lacking P/Q calcium channel activity. FASEB J 2001;15:1288–1290.
42. Uchitel OD, Protti DA, Sanchez V, et al. P-type voltage-dependent calcium channel mediates presynaptic calcium influx and transmitter release in mammalian synapses. Proc Natl Acad Sci U S A 1992;89:3330–3333.
43. Kaja S, van de Ven RC, Broos LA, et al. Characterization of acetylcholine release and the compensatory contribution of non-

Ca(v)2.1 channels at motor nerve terminals of leaner Ca(v)2.1-mutant mice. Neuroscience 2007;144:1278–1287.

44. Kaja S, van de Ven RC, Broos LA, et al. Gene dosage-dependent transmitter release changes at neuromuscular synapses of CACNA1A R192Q knockin mice are non-progressive and do not lead to morphological changes or muscle weakness. Neuroscience 2005;135:81–95.
45. Magleby KL, Stevens CF. The effect of voltage on the time course of end-plate currents. J Physiol 1972;223:151–171.
46. McLachlan EM, Martin AR. Non-linear summation of end-plate potentials in the frog and mouse. J Physiol 1981;311:307–324.
47. Zwingman TA, Neumann PE, Noebels JL, et al. Rocker is a new variant of the voltage-dependent calcium channel gene *Cacna1a*. J Neurosci 2001;21:1169–1178.
48. Gorji A. Spreading depression: a review of the clinical relevance. Brain Res Brain Res Rev 2001;38:33–60.
49. Solomon S. John Graham Senior Clinicians Award Lecture. Posttraumatic migraine. Headache 1998;38:772–778.
50. Hadjikhani N, Sanchez Del Rio M, Wu O, et al. Mechanisms of migraine aura revealed by functional MRI in human visual cortex. Proc Natl Acad Sci U S A 2001;98:4687–4692.
51. Bowyer SM, Aurora KS, Moran JE, et al. Magnetoencephalographic fields from patients with spontaneous and induced migraine aura. Ann Neurol 2001;50:582–587.
52. Whieldon JA, van Harreveld A. Cumulative effects of minimal cortical stimulation. Electroencephalogr Clin Neurophysiol 1950; 179:49–57.
53. Eikermann-Haerter K, Dileköz E, Kudo C, et al. Genetic and hormonal factors modulate spreading depression and transient hemiparesis in mouse models of familial hemiplegic migraine type 1. J Clin Invest 2009;119:99–109.
54. Takano T, Tian GF, Peng W, et al. Cortical spreading depression causes and coincides with tissue hypoxia. Nat Neurosci 2007;10: 754–762.
55. Gursoy-Ozdemir Y, Qiu J, Matsuoka N, et al. Cortical spreading depression activates and upregulates MMP-9. J Clin Invest 2004; 113:1447–1455.
56. Dreier JP, Jurkat-Rott K, Petzold GC, et al. Opening of the blood-brain barrier preceding cortical edema in a severe attack of FHM type II. Neurology 2005;64:2145–2147.
57. Hoebeek FE, Stahl JS, van Alphen AM, et al. Increased noise level of Purkinje cell activities minimizes impact of their modulation during sensorimotor control. Neuron 2005;45: 953–965.
58. Walter JT, Alviña K, Womack MD, et al. Decreases in the precision of Purkinje cell have making cause cerebellar dysfunction and ataxia. Nat Neurosci 2006;9:389–397.